

Type Ia Supernovae: Progenitors and Diversities

Ken'ichi Nomoto¹, Tatsuhiro Uenishi¹, Chiaki Kobayashi², Hideyuki Umeda¹, Takuya Ohkubo¹, Izumi Hachisu³, and Mariko Kato⁴

¹ Department of Astronomy, School of Science, University of Tokyo

² Max-Planck-Institut für Astrophysik, Garching

³ Department of Earth Science & Astronomy, University of Tokyo

⁴ Department of Astronomy, Keio University

Abstract. A key question for supernova cosmology is whether the peak luminosities of Type Ia supernovae (SNe Ia) are sufficiently free from the effects of cosmic and galactic evolution. To answer this question, we review the currently popular scenario of SN Ia progenitors, i.e., the single degenerate scenario for the Chandrasekhar mass white dwarf (WD) models. We identify the progenitor's evolution with two channels: (1) the WD+RG (red-giant) and (2) the WD+MS (near main-sequence He-rich star) channels. The strong wind from accreting WDs plays a key role, which yields important age and metallicity effects on the evolution.

We suggest that the variation of the carbon mass fraction $X(C)$ in the C+O WD (or the variation of the initial WD mass) causes the diversity of SN Ia brightness. This model can explain the observed dependence of SNe Ia brightness on the galaxy types. We then predict how SN Ia brightness evolves along the redshift (with changing metallicity and age) for elliptical and spiral galaxies. Such evolutionary effects along the redshift can be corrected as has been made for local SNe Ia.

We also touch on several related issues: (1) the abundance pattern of stars in dwarf spheroidal galaxies in relation to the metallicity effect on SNe Ia, (2) effects of angular momentum brought into the WD in relation to the diversities and the fate of double degenerates, and (3) possible presence of helium in the peculiar SN Ia 2000cx in relation to the sub-Chandrasekhar mass model.

1 Introduction

Relatively uniform light curves and spectral evolution of Type Ia supernovae (SNe Ia) have led to the use of SNe Ia as a "standard candle" to determine cosmological parameters. Whether a statistically significant value of the cosmological constant can be obtained depends on whether the peak luminosities of SNe Ia are sufficiently free from the effects of cosmic and galactic evolutions [20].

SNe Ia have been widely believed to be a thermonuclear explosion of a mass-accreting white dwarf (WD). However, the immediate progenitor binary systems have not been clearly identified yet [3]. In order to address the above questions regarding the nature of high-redshift SNe Ia, we need to identify the progenitors systems and examine the "evolutionary" effects (or environmental effects) on those systems [48].

Here we review several issues such as Chandra vs. sub-Chandra, double degenerates vs. single degenerate (AIC vs. SN Ia), C/O ratio, and rotation. For complete discussion, see earlier reviews on SN Ia progenitors [1,2,11,22,31–33].

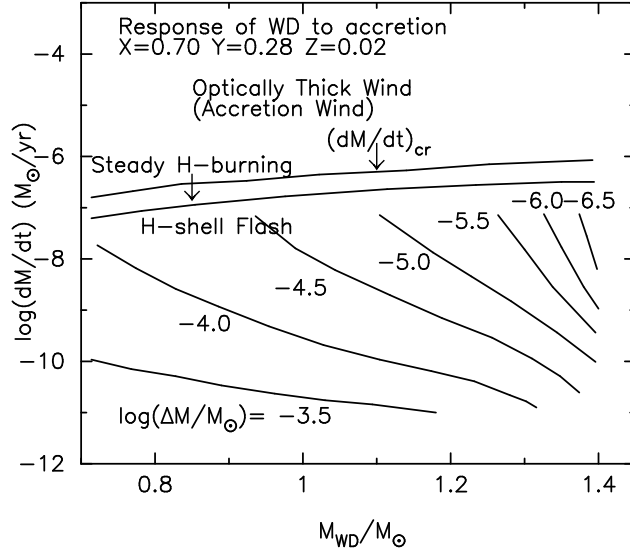


Fig. 1. The nature of hydrogen burning on accreting WD as functions of the WD mass and the accretion rate [25]. Above the steady burning regime, the WD blows optically thick wind [5].

2 Evolution of progenitor systems

Chandra vs. Sub-Chandra: There exist two models proposed as progenitors of SNe Ia: 1) the Chandrasekhar mass model, in which a mass-accreting carbon-oxygen (C+O) WD grows its mass M_{WD} up to the critical mass $M_{\text{Ia}} \simeq 1.37 - 1.38M_{\odot}$ near the Chandrasekhar mass and explodes as an SN Ia (e.g., [30,31]), and 2) the sub-Chandrasekhar mass model, in which an accreted layer of helium atop a C+O WD ignites off-center for a WD mass well below the Chandrasekhar mass (e.g., [1]). The early time spectra of the majority of SNe Ia are in excellent agreement with the synthetic spectra of the Chandrasekhar mass models, while the spectra of the sub-Chandrasekhar mass models are too blue to be comparable with the observations [12,34]. However, the peculiar SN Ia 2000cx might be the sub-Chandrasekhar mass explosion as will be discussed in §6.

Double Degenerates vs. Single Degenerate: For the evolution of accreting WDs toward the Chandrasekhar mass, two scenarios have been proposed: 1) a double degenerate (DD) scenario, i.e., merging of double C+O WDs [14,50], and 2) a single degenerate (SD) scenario, i.e., accretion of hydrogen-rich matter via mass transfer from a binary companion (e.g., [25,31]). The issue of DD vs. SD is still debated, although theoretical modeling has indicated that the merging of WDs leads to the accretion-induced collapse (AIC) rather than SN Ia explosion [40,42]. Whether the effect of rotation on accretion changes the conclusion on AIC vs. SN Ia will be discussed in §5.2.

2.1 White dwarf winds

In the SD Chandrasekhar mass model, a WD explodes as a SN Ia only when its rate of the mass accretion (\dot{M}) is in a certain narrow range (Fig. 1 [25,5]). In particular, if \dot{M} exceeds the critical rate \dot{M}_b , the accreted matter extends to form a common envelope [29]. Here \dot{M}_b is the rate at which steady burning can process the accreted hydrogen into helium as $\dot{M}_b \approx 0.75 \times 10^{-6} \left(\frac{M_{\text{WD}}}{M_{\odot}} - 0.40 \right) M_{\odot} \text{ yr}^{-1}$.

For $\dot{M} \gtrsim \dot{M}_b$, the strong peak of Fe opacity [15] drives the radiation-driven wind from the WD [7]. If the wind is sufficiently strong, the WD can avoid the formation of a common envelope and steady hydrogen burning increases its mass continuously at a rate \dot{M}_b by blowing the extra mass away in a wind. For $\dot{M} \lesssim 0.5 \dot{M}_b$, hydrogen shell burning becomes unstable to trigger weak shell flashes but still burns a large fraction of accreted hydrogen. Recurrent novae appear in the upper-right region of Fig. 1. In this way, strong winds from the accreting WD play a key role to increase the WD mass to M_{Ia} .

2.2 Progenitor binary systems

For the actual binary systems which grow M_{WD} to M_{Ia} , the following two systems are appropriate.

WD+RG system (Symbiotic system): This is a symbiotic binary system consisting of a WD and a low mass red-giant (RG) [7]. The immediate progenitor binaries in this symbiotic channel to SNe Ia may be observed as symbiotic stars, luminous supersoft X-ray sources, or recurrent novae like T CrB or RS Oph, depending on the wind status [5].

WD+MS system (Super-soft system): This is a system consisting of a mass-accreting WD and a lobe-filling, more massive, slightly evolved main-sequence or sub-giant star. In this scenario, a C+O WD is originated, not from an AGB star with a C+O core, but from a red-giant star with a helium core of $\sim 0.8 - 2.0 M_{\odot}$. The helium star, which is formed after the first common envelope evolution, evolves to form a C+O WD of $\sim 0.8 - 1.1 M_{\odot}$ with transferring a part of the helium envelope onto the secondary main-sequence star [6].

A part of the progenitor systems are identified as the luminous supersoft X-ray sources [49] during steady H-burning (but without wind to avoid extinction), or the recurrent novae like U Sco if H-burning is weakly unstable [5]. Actually these objects are characterized by the accretion of helium-rich matter.

Realization frequency: The rate of SNe Ia originating from these channels in our Galaxy is estimated with equation (1) of [14]. The realization frequencies of SNe Ia through the WD+RG and WD+MS channels are estimated as $\sim 0.0017 \text{ yr}^{-1}$ (WD+RG) and $\sim 0.001 \text{ yr}^{-1}$ (WD+MS), respectively. The total SN Ia rate of the WD+MS/WD+RG systems becomes $\sim 0.003 \text{ yr}^{-1}$, which is close enough to the inferred rate of our Galaxy.

2.3 Metallicity dependence of type Ia supernovae

The optically thick winds are driven by a strong peak of OPAL opacity due to iron lines. Thus the wind velocity v_w is lower for lower $[\text{Fe}/\text{H}]$. The SN Ia regions are much smaller for lower metallicity, and very few SN Ia occurs at $[\text{Fe}/\text{H}] \leq -1.1$ in this model. It is possible to test such metallicity effects on SNe Ia with the chemical evolution of galaxies.

In the one-zone uniform model for the chemical evolution of the solar neighborhood, the heavy elements in the metal-poor stars originate from the mixture of the SN II ejecta of various progenitor masses. The abundances averaged over the progenitor masses of SNe II predicts $[\text{O}/\text{Fe}] \sim 0.45$ (e.g., [44]). Later SNe Ia start ejecting mostly Fe, so that $[\text{O}/\text{Fe}]$ decreases to ~ 0 around $[\text{Fe}/\text{H}] \sim 0$. The low-metallicity inhibition of SNe Ia predicts that the decrease in $[\text{O}/\text{Fe}]$ starts at $[\text{Fe}/\text{H}] \sim -1$. Such an evolution of $[\text{O}/\text{Fe}]$ well explains the observations [18,19].

We should note that some anomalous stars have $[\text{O}/\text{Fe}] \sim 0$ at $[\text{Fe}/\text{H}] \lesssim -1$. The presence of such stars, however, is not in conflict with the metallicity dependence of SNe Ia, but can be understood as follows: The formation of such anomalous stars (and the diversity of $[\text{O}/\text{Fe}]$ in general) indicates that the interstellar materials were not uniformly mixed but contaminated by only a few SNe II (or even single SN II) ejecta. The Fe and O abundances produced by a single SN II vary depending mainly on the mass of the progenitor. Relatively smaller mass SNe II ($13 - 15 M_\odot$) and higher explosion energies tend to produce $[\text{O}/\text{Fe}] \sim 0$ [44,46]. Those metal-poor stars with $[\text{O}/\text{Fe}] \sim 0$ may be born from the interstellar medium polluted by such SNe II. Alternatively, such stars were born in nearby dwarf spheroidal galaxies and captured by our Galaxy (see below).

2.4 Abundances in dwarf spheroidal galaxies

The chemical abundances of individual stars in local dwarf spheroidal galaxies (dSph) have been measured (e.g., [43] for recent observations and references therein). These stars have $[\text{Fe}/\text{H}] < -1$ but the ratios between the α elements and Fe are found to be as low as $[\alpha/\text{Fe}] \sim 0$ being significantly lower than the metal-poor halo-stars in our Galaxy. If the low $[\alpha/\text{Fe}]$ was due to the Fe-enrichment by SNe Ia, it implies that SNe Ia appeared in low metallicity environment, which may be difficult to explain with the metallicity dependent SN Ia model.

However, it is possible to produce such low $[\alpha/\text{Fe}]$ with core-collapse SNe. As discussed above, yields from $13-15 M_\odot$ stars have low (even sub-solar) $[\alpha/\text{Fe}]$. Thus if IMF in those dwarf spheroidal galaxies is steep enough or the upper limit mass of core-collapse SNe is truncated around $20 M_\odot$ [43], the contribution of $13-15 M_\odot$ stars could be significantly larger than in our Galaxy. Also it is possible that some fraction of AGB stars suffers less mass loss because of low metallicity, thus growing degenerate C+O cores to the Chandrasekhar mass before losing entire envelopes. If this is the case, those metal-poor AGB stars undergo SN Ia-like explosions (SN I+1/2). If the mass range is very narrow, say $\sim 7.5-8.0 M_\odot$, SNe I+1/2 do not affect $[\text{O}/\text{Fe}]$ for our Galaxy if integrated over the Salpeter IMF up to $50 M_\odot$ [28]. However, if IMF is steeper or the upper-mass limit is

lower, contributions of SNe I+1/2 and 13-15 M_{\odot} stars are larger, thus reducing $[\alpha/\text{Fe}]$.

The abundance patterns in dSph as well as some Damped Lyman- α systems can provide important constraint on the progenitor mass ranges of SNe Ia, SNe I+1/2, and SNe II. Also the appearance of SNe Ia in more metal-rich regions of dSph may not be impossible in view of spatial inhomogeneity.

3 The origin of diversity of type Ia supernovae

There are some observational indications that SNe Ia depend on the type of the host galaxies. The most luminous SNe Ia seem to occur only in spiral galaxies, while both spiral and elliptical galaxies are hosts for dimmer SNe Ia. Thus the mean peak brightness is dimmer in ellipticals than in spiral galaxies [9]. Also the SNe Ia rate per unit luminosity at the present epoch is almost twice as high in spirals as in ellipticals [4].

Umeda et al. [48] suggested that the variation of the C/O ratio is the main cause of the variation of SNe Ia brightness, with larger C/O ratio yielding brighter SNe Ia. Here we will show that the C/O ratio depends indeed on the metallicity and age of the companion of the WD, and that the model can explain most of the observational trends discussed above. We then make some predictions about the brightness of SN Ia at higher redshift.

3.1 C/O ratio in white dwarf progenitors

The C/O ratio in C+O WDs depends primarily on the main-sequence mass of the WD progenitor and on metallicity. The most important metallicity effect is that the radiative opacity is smaller for lower Z . Therefore, a star with lower Z is brighter, thus having a shorter lifetime than a star with the same mass but higher Z . In this sense, the effect of reducing metallicity for these stars is almost equivalent to increasing a stellar mass.

For stars with larger masses and/or smaller Z , the luminosity is higher at the same evolutionary phase. With a higher nuclear energy generation rate, these stars have larger convective cores during H and He burning, thus forming larger He and C-O cores.

According to the evolutionary calculations for 3–9 M_{\odot} stars [47], the C/O ratio and its distribution are determined in the following evolutionary stages of the close binary.

(1) At the end of central He burning in the 3–9 M_{\odot} primary star, $C/O < 1$ in the convective core. The mass of the core is larger for more massive stars.

(2) After central He exhaustion, the outer C+O layer grows via He shell burning, where $C/O \gtrsim 1$ [47].

(3a) If the primary star becomes a red giant (case C evolution), it then undergoes the second dredge-up, forming a thin He layer, and enters the AGB phase. The C+O core mass, M_{CO} , at this phase is larger for more massive stars. For a larger M_{CO} the total carbon mass fraction is smaller.

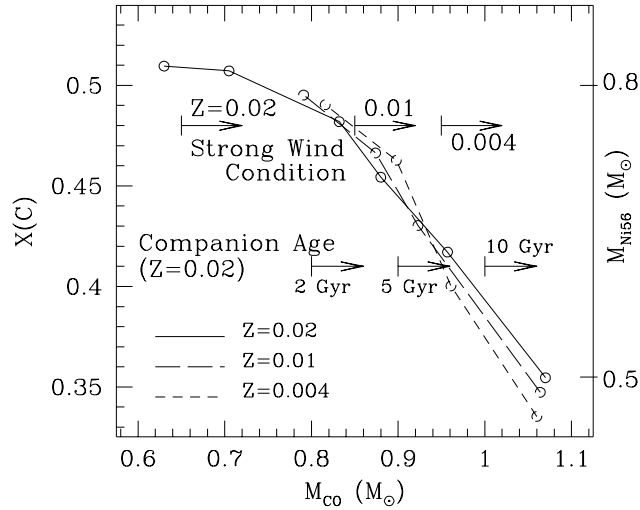


Fig. 2. The total ^{12}C mass fraction included in the convective core of mass, $M = 1.14M_{\odot}$, just before the SN Ia explosion as a function of the C+O core mass before the onset of mass accretion, M_{CO} . The lower bounds of M_{CO} obtained from the age effects and the conditions for strong wind to blow are also shown by arrows [48].

(3b) When it enters the AGB phase, the star greatly expands and is assumed here to undergo Roche lobe overflow (or a super-wind phase) and to form a C+O WD. Thus the initial mass of the WD, $M_{\text{WD},0}$, in the close binary at the beginning of mass accretion is approximately equal to M_{CO} .

(4a) If the primary star becomes a He star (case BB evolution), the second dredge-up in (3a) corresponds to the expansion of the He envelope.

(4b) The ensuing Roche lobe overflow again leads to a WD of $M_{\text{WD},0} = M_{\text{CO}}$.

(5) After the onset of mass accretion, the WD mass grows through steady H burning and weak He shell flashes, as described in the WD wind model. The composition of the growing C+O layer is assumed to be C/O=1.

(6) The WD grows in mass and ignites carbon when its mass reaches $M_{\text{Ia}} = 1.367M_{\odot}$, as in the model C6 [30]. Carbon burning grows into a deflagration for a central temperature of 8×10^8 K and a central density of 1.47×10^9 g cm $^{-3}$. At this stage, the convective core extends to $M_r = 1.14M_{\odot}$ and the material is mixed almost uniformly (model C6).

Figure 2 shows the carbon mass fraction $X(\text{C})$ in the convective core of this pre-explosive WD, as a function of metallicity (Z) and initial mass of the WD before the onset of mass accretion, M_{CO} . We note:

1) $X(\text{C})$ is smaller for larger $M_{\text{CO}} \simeq M_{\text{WD},0}$.

2) The dependence of $X(\text{C})$ on metallicity is small when plotted against M_{CO} , even though the relation between M_{CO} and the initial stellar mass depends sensitively on Z [47].

3.2 Brightness of type Ia supernovae and the C/O ratio

In the Chandrasekhar mass models for SNe Ia, brightness of SNe Ia is determined mainly by the mass of ^{56}Ni synthesized ($M_{\text{Ni}56}$). Observational data suggest that $M_{\text{Ni}56}$ for most SNe Ia lies in the range $M_{\text{Ni}56} \sim 0.4 - 0.8M_{\odot}$ (e.g., [24]).

Here we postulate that $M_{\text{Ni}56}$ and consequently brightness of a SN Ia increase as the progenitors' C/O ratio increases (and thus $M_{\text{WD},0}$ decreases). As illustrated in Figure 2, the range of $M_{\text{Ni}56} \sim 0.5 - 0.8M_{\odot}$ is the result of an $X(\text{C})$ range $0.35 - 0.5$, which is the range of $X(\text{C})$ values of our progenitor models. The $X(\text{C}) - M_{\text{Ni}56} - M_{\text{WD},0}$ relation we adopt is still only a working hypothesis, which needs to be proved from studies of the turbulent flame during explosion (e.g., [11]).

3.3 Metallicity and age effects

Assuming the relation between $M_{\text{Ni}56}$ and $X(\text{C})$ given in Figure 2, the model predicts the absence of brighter SNe Ia in lower metallicity environment.

In this model, the age of the progenitor system also constrains the range of $X(\text{C})$ in SNe Ia. In the SD scenario, the lifetime of the binary system is essentially the main-sequence lifetime of the companion star, which depends on its initial mass M_2 . In order for the WD mass to reach M_{Ia} , the donor star should transfer enough material at the appropriate accretion rates. The donors of successful SN Ia cases are divided into two categories: one is composed of slightly evolved main-sequence stars with $M_2 \sim 1.7 - 3.6M_{\odot}$ (for $Z=0.02$), and the other of red-giant stars with $M_2 \sim 0.8 - 3.1M_{\odot}$ (for $Z=0.02$) [17].

If the progenitor system is older than 2 Gyr, it should be a system with a donor star of $M_2 < 1.7M_{\odot}$ in the red-giant branch. Systems with $M_2 > 1.7M_{\odot}$ become SNe Ia in a time shorter than 2 Gyr. Likewise, for a given age of the progenitor system, M_2 must be smaller than a limiting mass. This constraint on M_2 can be translated into the presence of a minimum M_{CO} for a given age, as follows: For a smaller M_2 , i.e. for the older system, the total mass which can be transferred from the donor to the WD is smaller. In order for M_{WD} to reach M_{Ia} , therefore, the initial mass of the WD, $M_{\text{WD},0} \simeq M_{\text{CO}}$, should be larger. This implies that the older system should have larger minimum M_{CO} as indicated in Figure 2. Using the $X(\text{C})$ - M_{CO} and $M_{\text{Ni}56}$ - $X(\text{C})$ relations (Fig. 2), we conclude that WDs in older progenitor systems have a smaller $X(\text{C})$, and thus produce dimmer SNe Ia.

3.4 Morphology of the host galaxies

Among the observational indications which can be compared with our model is the possible dependence of the SN brightness on the morphology of the host galaxies. Hamuy et al. [9] found that the most luminous SNe Ia occur in spiral galaxies, while both spiral and elliptical galaxies are hosts to dimmer SNe Ia. Hence, the mean peak brightness is lower in elliptical than in spiral galaxies.

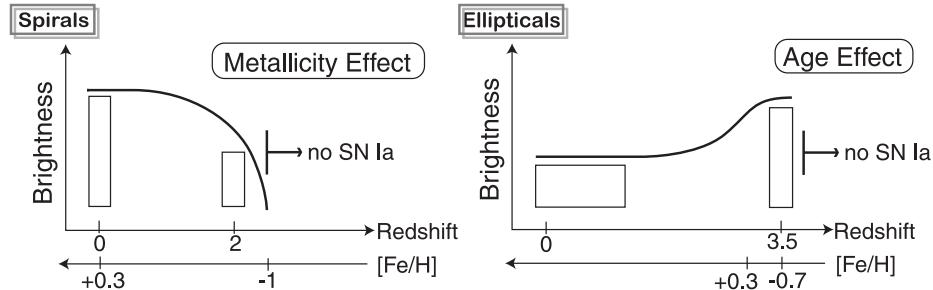


Fig. 3. Illustration of the predicted variation in SN Ia brightness with redshift.

In our model, this property is simply understood as the effect of the different age of the companion. In spiral galaxies, star formation occurs continuously up to the present time. Hence, both WD+MS and WD+RG systems can produce SNe Ia. In elliptical galaxies, on the other hand, star formation has long ended, typically more than 10 Gyr ago. Hence, WD+MS systems can no longer produce SNe Ia. Since a WD with smaller M_{CO} is assumed to produce a brighter SN Ia (larger M_{Ni56}), our model predicts that dimmer SNe Ia occur both in spirals and in ellipticals, while brighter ones occur only in spirals. The mean brightness is smaller for ellipticals and the total SN Ia rate per unit luminosity is larger in spirals than in ellipticals. These properties are consistent with observations.

3.5 Evolution of type Ia supernovae at high redshift

Our model predicts that when the progenitors belong to an old population, or to a low metal environment, the number of very bright SNe Ia is small, so that the variation in brightness is also smaller, which is shown in Figure 3. In spiral galaxies, the metallicity is significantly smaller at redshifts $z \gtrsim 1$, and thus both the mean brightness of SNe Ia and its range tend to be smaller (Fig. 3). At $z \gtrsim 2$ SNe Ia would not occur in spirals at all because the metallicity is too low. In elliptical galaxies, on the other hand, the metallicity at redshifts $z \sim 1 - 3$ is not very different from the present value. However, the age of the galaxies at $z \simeq 1$ is only about 5 Gyr, so that the mean brightness of SNe Ia and its range tend to be larger at $z \gtrsim 1$ than in the present ellipticals because of the age effect.

We note that the variation of $X(C)$ is larger in metal-rich nearby spirals than in high redshift galaxies. Therefore, if $X(C)$ is the main parameter responsible for the diversity of SNe Ia, and if the light curve shape (LCS) method is confirmed by the nearby SNe Ia data [38,8], the LCS method can also be used to determine the absolute magnitude of high redshift SNe Ia.

Here we consider the metallicity effects only on the C/O ratio; this is just to shift the main-sequence mass - $M_{\text{WD},0}$ relation, thus resulting in no important evolutionary effect. However, some other metallicity effects could give rise to evolution of SNe Ia between high and low redshifts (i.e., between low and high metallicities) (see, e.g., [33]).

4 Rotation

The accreting WD gains angular momentum from the rotating disk in addition to the mass, thus rotating faster and faster. Rapid rotation of a WD affects its limiting mass and final structure. The effects of rotation on the evolution of accreting WDs have been studied mostly with 1D approximate models (e.g., [53,36,41]).

4.1 Diversity and rotation

Uenishi et al. [45] have calculated the axisymmetric structure of *uniformly* rotating WDs and followed the evolutionary sequence in the total angular momentum J and the WD mass M (Fig. 4). Here accreting gas is supposed to obey Keplerian rotation law and gives its angular momentum to the WD. The almost straight lines show the evolutionary tracks of the accreting WDs starting from the initial masses of $0.6 M_{\odot}$, $0.8 M_{\odot}$, and $1.07 M_{\odot}$, respectively. After gaining $\sim 0.1 M_{\odot}$, the WDs reach the critical rotation at the upper edge of the $J - M$ diagram where the equatorial centrifugal force is equal to the gravity.

For WDs which have reached the critical rotation, Paczyński [35] and Pooham & Narayan [37] found a solution that permits the WD to accrete without becoming secularly unstable. In such a solution, the angular momentum is transported backwards from the WD to the disk while the mass of the WD increases. Then the WD evolves along the upper envelope in the $J - M$ plane and eventually explodes at the upper-right corner. (Along the right edge of the diagram, the central density of WDs is $2 \times 10^9 \text{ g cm}^{-3}$ where carbon is ignited.) Then all the rapidly rotating WDs explode with the same (M, J) . In other words, *uniform* rotation leads to the uniformity rather than the diversity of SNe Ia.

However, rotation could produce the diversity of SNe Ia in the following way. The uniform rotation is realized if the timescale of angular momentum transport in the WDs is much shorter than the accretion time scale. If the angular momentum transport is much slower, then the initially non-rotating part of the WD may remain non-rotating, while the accreted outer part of the WD rotates fast and reaches the critical rotation. When the WD reaches the carbon ignition at the limiting mass, the angular momentum brought into the WD is larger (smaller) for smaller (larger) M_0 . The WD with smaller M_0 grows to larger M_{fin} at the explosion. Although $M_{\text{fin}} \sim 1.45 M_{\odot}$ are not so different from each other, larger M_{fin} could produce brighter SNe Ia.

Also the distribution of the angular velocity is different, i.e., the non-rotating core is smaller (larger) for smaller (larger) M_0 . Such a difference might affect the flame propagation and lead to different amount of ^{56}Ni .

If the WD with smaller M_0 produce a brighter SN Ia with the effect of rotation, the upper limit of SNe Ia brightness is higher in spirals than in ellipticals. SNe Ia in spirals can originate from WDs with a wide range of M_0 , thus having a large dispersion of brightness than those in ellipticals. This could explain the observation that the most luminous SNe Ia appear to be observed only in spirals, while dimmer SNe Ia are observed in both spirals and ellipticals.

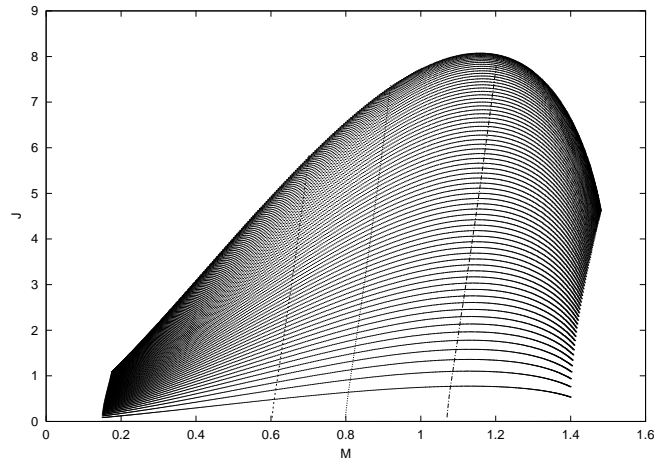


Fig. 4. The evolutionary track in the total angular momentum J (10^{49} erg sec) and the WD mass M (M_{\odot}) of uniformly rotating WDs starting from the initial masses of $0.6 M_{\odot}$, $0.8 M_{\odot}$, and $1.07 M_{\odot}$ [45].

4.2 Rotation and rapid accretion in merging white dwarfs

Nomoto & Iben [27] and Saio & Nomoto [40] have simulated the merging of double WDs in 1D and shown that the rapidly accreting WDs undergo off-center carbon ignition if $\dot{M} \gtrsim 2 \times 10^{-6} M_{\odot} \text{ yr}^{-1}$ because of compressional heating. Afterwards carbon flame propagates inward through the center and converts C+O into O+Ne+Mg. Then the final outcome is most likely accretion-induced collapse rather than SNe Ia.

Recently Piersanti et al. [36] calculated the evolution of WDs with rotation in 1D approximation and argued that the lifting effect of rotation reduces compressional heating, and the WD could avoid off-center carbon ignition and reach the central carbon ignition to produce SNe Ia. However, they did not follow the accretion after the critical rotation is reached because the backward transport of angular momentum to the disk was not taken into account.

Saio & Nomoto [41] have also calculated the accretion of C+O onto the C+O WD with rotation for various timescale of angular momentum transport in 1D approximation. The outermost layer of the accreting WD quickly reaches the critical rotation as in Figure 4. Afterwards, the angular momentum is transported backward to disk and accretion continues. For $\dot{M} \gtrsim 4 \times 10^{-6} M_{\odot} \text{ yr}^{-1}$, off-center carbon burning is ignited prior to the central C-ignition. Thus the lifting effect of rotation increases the critical accretion rate for the occurrence of off-center C-ignition by a factor of ~ 2 compared with the non-rotating case, but the basic conclusion is the same as non-rotating case, i.e., the accretion-induced collapse is the most likely outcome in the DD scenario [40].

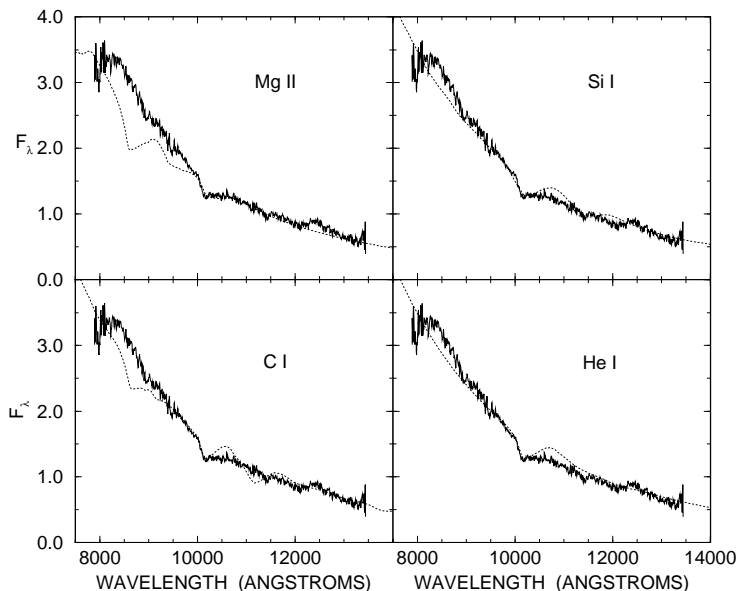


Fig. 5. The average of two infrared spectra of SN 2000cx obtained by Rudy et al.[39] at the Lick Observatory on 2000 July band (solid lines) is compared with four synthetic spectra (dotted lines), each of which contain lines of only one ion [10].

5 SN 2000cx

Supernova 2000cx was a very well observed SN Ia that in certain respects resembled the peculiar “powerful” SN 1991T, but also showed some photometric and spectroscopic characteristics that are unprecedented among well observed SNe Ia (Li et al. [21]; hereafter L01).

5.1 Infrared spectra

Rudy et al. ([39]; hereafter R02) obtained infrared spectra covering the range 0.8 to 2.5 μm , 6 and 5 days before optical maximum. They attributed an absorption feature near 1.0 μm to Mg II $\lambda 10926$. Hatano et al. [10] have used spectrum code SYNOW and found that the absorption feature is most likely due to He I $\lambda 10830$. The presence of helium would have important implications for models.

In Figure 5 the infrared spectrum [39] is compared with four synthetic spectra, each containing lines of only one ion. The synthetic spectra have $T_{\text{bb}} = T_{\text{exc}} = 12,000$ K and $v_{\text{phot}} = 22,000$ km s $^{-1}$ (Mg II), 16,000 km s $^{-1}$ (C I), and 20,000 km s $^{-1}$ (Si I and He I).

Mg II $\lambda 10926$ has been considered as a possible identification for the absorption feature by R02. However, the upper left panel of Figure 5 shows that when $\lambda 10926$ is strong enough to account for the 1.0 μm absorption, other Mg II lines produce unwanted absorptions near 8600 \AA ($\lambda 9226$) and 9400 \AA ($\lambda 9632$). In

LTE $\lambda 9226$ has a larger optical depth than $\lambda 10926$ for any reasonable excitation temperature. It is unlikely that Mg II is responsible for the $1.0 \mu\text{m}$ feature.

The lower left panel of Figure 5 shows that C I, with $\lambda 10695$ producing the $1.0 \mu\text{m}$ absorption, has a similar problem of unwanted features, due to $\lambda 9055$ and $\lambda 11755$. The upper right panel shows that a group of Si I lines (mainly a multiplet at $\lambda 10790$) fit the $1.0 \mu\text{m}$ feature without severe problems; a feature due to $\lambda 12047$ is from the same lower level and is stronger, but one might argue that it is possibly present, blended with other lines, in the observed spectrum. However, unless the level of ionization in SN 2000cx was much lower at the epoch of the infrared spectrum than it was at the time of the first optical spectrum, just a few days later, Si I lines would not be expected. Finally, the lower right panel of Figure 5 shows that He I $\lambda 10830$, with a optical depth at the photosphere of 0.9, can account for the $1.0 \mu\text{m}$ feature without causing any obvious problems. By this process of elimination, Hatano et al. [10] find that the most likely identification of the $1.0 \mu\text{m}$ feature in SN 2000cx is He I $\lambda 10830$. The evidence for helium in SN 2000cx, although not conclusive, is strong enough to be taken seriously.

5.2 Sub-Chandrasekhar mass model

Both L01 and R02 suggest a delayed detonation as a favorable model for SN 2000cx. In particular, R02 argued that the $1.0 \mu\text{m}$ feature is due to Mg II and the presence of such high velocity Mg as $\gtrsim 20,000 \text{ km s}^{-1}$ supports the delayed detonation model. However, this argument does not hold if the $1.0 \mu\text{m}$ feature is due to He I. Rather the delayed detonation models do not contain such high velocity He (e.g., [16]).

The presence of He, instead, may suggest the sub-Chandrasekhar model for SN 2000cx. In the sub-Chandrasekhar mass models, the He detonation in the outer He layer synthesizes mostly ^{56}Ni but significant amount of He is also present due to strong α -rich freezeout [26,23,51,32]. The velocities of He are $\sim 11,000 - 14,000 \text{ km s}^{-1}$ near the bottom of the He layer and $\sim 25,000 - 30,000 \text{ km s}^{-1}$ near the surface, depending on M_{WD} and the mass of the He layer (M_{He}). The He velocities and the ^{56}Ni mass of SN 2000cx could be consistent with the model with relatively large M_{WD} and M_{He} . In the outer detonated layers, little Si is produced, which is also consistent with the weak Si features of SN 2000cx.

The presence of high velocity He with ^{56}Ni (and little Si) is also seen in the late detonation model W7DHE of the Chandrasekhar mass white dwarf [52]. The explosion of this type would occur for slower accretion than the sub-Chandrasekhar mass explosion [25].

References

1. Arnett, W. D. 1996, *Nucleosynthesis and Supernovae* (Princeton Univ. Press)
2. Branch, D. 1998, *ARA&A*, 1998, 36, 17
3. Branch, D., Livio, M., Yungelson, L., Boffi, F., Baron, E. 1995, *PASP*, 107, 717
4. Cappellaro, E. et al. 1997, *A&A*, 322, 431

5. Hachisu, I., & Kato, M., 2001, *ApJ*, 558, 323
6. Hachisu, I., Kato, M., Nomoto, K., & Umeda, H. 1999a, *ApJ*, 519, 314
7. Hachisu, I., Kato, M., & Nomoto, K. 1999b, *ApJ*, 522, 487
8. Hamuy, M., et al. 1995, *AJ*, 109, 1
9. Hamuy, M., Phillips, M.M., Schommer, R., & Suntzeff, N.B., 1996, *AJ*, 112, 2391
10. Hatano, K., Branch, D., Nomoto, K., Baron, E. 2002, in preparation
11. Hillebrandt W., & Niemeyer J.C. 2000, *ARA&A*, 38, 191
12. Höflich, P., & Khokhlov, A., 1996, *ApJ*, 457, 500
13. Höflich, P., Wheeler, J. C., & Thielemann, F. -K., 1998, *ApJ*, 495, 617
14. Iben, I. Jr., & Tutukov, A. V. 1984, *ApJS*, 54, 335
15. Iglesias, C. A., & Rogers, F. 1993, *ApJ*, 412, 752
16. Iwamoto, K., Brachwitz, F., Nomoto, K., et al. 1999, *ApJS*, 125, 439
17. Kobayashi, C., & Nomoto, K. 2002, in this volume, 379
18. Kobayashi, C., Tsujimoto, T., Nomoto, K., et al. 1998, *ApJ*, 503, L155
19. Kobayashi, C., Tsujimoto, T., & Nomoto, K. 2000, *ApJ*, 539, 26
20. Leibundgut, B. 2001, *ARA&A*, 39, 67
21. Li, W. D. et al. 2001, *PASP*, 113, 1178 (L01)
22. Livio, M. 2000, in *Type Ia Supernovae*, ed. J. Niemeyer (Univ. Chicago press), 33
23. Livne, E., & Arnett, W. D. 1995, *ApJ*, 452, 62
24. Mazzali, P. A. & Lucy, L. B. 1998, *MNRAS*, 295, 428
25. Nomoto, K. 1982a, *ApJ*, 253, 798
26. Nomoto, K. 1982b, *ApJ*, 257, 780
27. Nomoto, K., & Iben, I. Jr. 1985, *ApJ*, 297, 531
28. Nomoto, K., Shigeyama, T., & Tsujimoto, T. 1991, in *IAU Symp. 145, Evolution of Stars: The Photospheric Abundance Connection*, ed. G. Michaud (Kluwer), 21
29. Nomoto, K., Nariai, K., & Sugimoto, D. 1979, *PASJ*, 31, 287
30. Nomoto, K., Thielemann, F. -K., & Yokoi, K., 1984, *ApJ*, 286, 644
31. Nomoto, K., Yamaoka, H., Shigeyama, T., Kumagai, S., Tsujimoto, T. 1994, in *Supernovae, Les Houches Session LIV*, ed. S. Bludman (North-Holland), 199
32. Nomoto, K. et al. 1997a, *Science*, 276, 1378; 1997b, in *Thermonuclear Supernovae*, eds. P.Ruiz-Lapuente et al. (Dordrecht: Kluwer), 349
33. Nomoto, K. 2000, in *Type Ia Supernovae*, ed. J. Niemeyer (Univ Chicago), 63
34. Nugent, P., Baron, E., Branch, D., Fisher, A., Hauschildt, P. 1997, *ApJ*, 485, 812
35. Paczyński, B. 1990, *ApJ*, 370, 597
36. Piersanti, L., Gagliardi, S., Iben, I., Jr., Tornambe, A. 2003, *ApJ*, 583, 885
37. Popham, R., & Narayan, R. 1990, *ApJ*, 370, 604
38. Riess, A. G., Press, W. H., & Kirshner, R. P. 1995, *ApJ*, 438, L17
39. Rudy, R.J., Lynch, D.K., Mazuk, S., et al. 2002, *ApJ*, 565, 413 (R02)
40. Saio, H., & Nomoto, K. 1998, *ApJ*, 500, 388; 1985, *A&A*, 150, L21
41. Saio, H., & Nomoto, K. 2002, in preparation
42. Segretain, L., Chabrier, G., & Mochkovitch, R. 1997, *ApJ*, 481, 355
43. Shetrone, M., Venn, K., Tolstoy, E., et al. 2003, *AJ*, 125, 684
44. Thielemann, F.-K., Nomoto, K., & Hashimoto, M. 1996, *ApJ*, 460, 408
45. Uenishi, T., Nomoto, K., & Hachisu, I. 2002, in *New Trends in Theoretical and Observational Cosmology*, ed. K. Sato (Tokyo: Universal Acad. Press), 129
46. Umeda, H., & Nomoto, K. 2002, *ApJ*, 565, 385
47. Umeda, H., Nomoto, K., Yamaoka, H., & Wanajo, S. 1999a, *ApJ*, 513, 861
48. Umeda, H., Nomoto, K., Kobayashi, C., Hachisu, I., Kato, M. 1999b, *ApJ*, 522, L43
49. van den Heuvel, E.P.J., Bhattacharya, D., Nomoto, K., et al. 1992, *A&A*, 262, 97
50. Webbink, R. F. 1984, *ApJ*, 277, 355
51. Woosley, S. E., & Weaver, T. A. 1994, *ApJ*, 423, 371
52. Yamaoka, H., Nomoto, K., Shigeyama, T., Thielemann, F.-K. 1992, *ApJ*, 393, L55
53. Yoon, S.-C., Langer, N., & Scheithauer, S. 2002, *A&A*, submitted